# Deep Feature Extraction with SVM Classification: A Robust Framework for Lung Cancer Detection in Histological Images

Jayaprakash B[1*]

[1*] Department of Computer Science and IT, JAIN (Deemed-to-be University), Bengaluru, India
[1]b.jayaprakash@jainuniversity.ac.in.

**Abstract.** Lung cancer is the largest cause of cancer-related death globally, necessitating the urgent development of reliable and rapid diagnostic tools to aid clinical decision-making. Although deep learning models like DenseNet121 and ResNet-50 perform well in image-based classification tasks, their high tuning complexity, overfitting risk, and reliance on large-scale datasets restrict their usefulness in tiny and high-dimensional biomedical situations. Existing VGG16- and SVM-based studies have also shown promise, but most have been constrained by small sample numbers, insufficient hyperparameter optimization, and a dependence on single-modality data, pre-venting them from properly capturing the biological heterogeneity of lung cancer. To overcome these constraints, this paper offers a new Dandelion Optimizer (DO)-based hybrid VGG16-SVM architecture for multimodal lung cancer classification. The proposed system uses pretrained VGG16 for deep feature extraction because its uniform neural architecture retains fine-grained histopathological textures and allows for reliable multi-scale representation learning. SVM is utilized as a classifier to successfully handle high-dimensional feature spaces and increase generalization under limited-data situations, whereas DO is used to optimize critical SVM hyperparameters for better decision-boundary creation. Images from the LungHist700 dataset were preprocessed using Macenko stain normalization, background eradication, augmentation, and patch-level ex-traction at 224 × 224 resolution. The retrieved 512-dimensional deep features were combined with transcriptomic, proteomic, and clinical data to create a structured multimodal picture. This study's originality resides in the integration of multimodal biological data with a decoupled VGG16-SVM architecture and DO-based optimization, which allows for better modelling of nonlinear interactions and cancer heterogeneity while improving robustness, interpretability, and generalization. Experimental findings show that the proposed framework outperforms conventional and unimodal baselines, with 96.94% accuracy, 97.11% precision, 98.95% recall, a 98.02% F1-score, and an AUC of 0.99. These results validate the proposed model as a scalable, interpretable, and high-performance framework for lung cancer classification, laying the groundwork for future clinically applicable AI-based diagnostic tools.

**Keywords:** Lung cancer, Histopathology, VGG16, Support Vector Machine, Dandelion Optimizer (DO), Deep learning, Stain normalization, Multimodal fusion, Digital pathology.


B. Singh et al. (eds.), *Proceedings of the International Conference on Advances in Computing Technology and Artificial Intelligence (COMPUTATIA 2026)*, Atlantis Highlights in Intelligent Systems 18,
https://doi.org/10.2991/978-94-6239-713-2_2

# 1 Introduction

Worldwide, 1.8 million people will lose their lives to lung cancer in 2020, while an additional 2.2 million will be diagnosed with the disease [1],[2]. In spite of the recent advancements via the identification and management of lung cancer, the prognosis rate after five years of diagnosis is still very low. The diverse tumor morphologies and the difficulties in making a prompt diagnosis of lung cancer are the main factors contributing to its poor survival rate [3]. The precise and timely identification classification of lung cancer subtypes provides the groundwork for developing personalized treatment methods which improve patient outcomes. There are two main subtypes of lung cancer: small-cell and non-small-cell [4]. The standard diagnostic methods require both histopathological testing and expert evaluations from medical professionals. The diagnostic methods require extensive work but they still maintain risk of different observers producing varying results [5]. Computer-aided diagnostic techniques have evolved in recent years into a valuable solution that effectively overcomes existing limitations through their ability to offer standardized and reliable evaluation methods for both radiographic and histological images [6],[7]. Deep learning algorithms have changed image diagnostic procedures through their implementation of convolutional neural networks [8],[9],[10]. The algorithms demonstrate high performance be-because they can extract features and classify information with precise accuracy. The ability to learn hierarchical structures of information from raw pixel input is what makes VGG16, ResNet, as well as Inception architectures so useful in medical imaging [11]. The design of VGG16 uses consistent architectural elements that implemented small convolutional filters. This design choice enables VGG16 to effectively capture nearby visual patterns while requiring minimal processing resources. The A team of Oxford University scholars studying visual geometry created architecture.

CNN models demonstrate strong performance throughout the complete image classification process while researchers focus their attention on hybrid methods that divide feature extraction from classification. The common method employs CNNs for feature extraction Several study groups use sup-port vector machines (SVMs) to take use of SVMs' high-dimensional space handling capabilities [12]. Multiple research investigations have tested whether traditional machine learning classifiers combined with CNN-based feature extraction methods can effectively detect lung cancer [13]. The research demonstrates that optimized SVMs outperform fully connected layers during specific tasks which use publicly available CT scan datasets [14]. The results of the experiments show that CNNs achieve superior representation learning performance through their learning abilities while SVMs demonstrate optimal performance for boundary detection tasks which require minimal training data [7]. The performance of SVMs in hybrid models may be significantly influenced by kernel function and regularization parameter choices. Better classification performance needs hyperparameter optimization which is essential for achievement. The Grid-Search CV method provides an effective way to select optimal parameter combinations which work best with SVM classifiers [15]. The approach employs a systematic tuning process which uses cross-validation to determine optimal parameters while safeguarding against overfitting and ensuring accurate performance on unseen data [16]. The application of GridSearchCV for SVM parameter

optimization in previous medical imaging studies resulted in substantial performance improvements which included a seven per-cent ac-curacy increase for breast histopathology categorization when compared to the best default parameter settings [17]. The research studies that follow this method for lung cancer classification Using deep characteristics has been undertaken by a meagre handful of scholars [18]. There is room for improvement in the current technology, which displays a balance. The primary obstacle presents itself through two problems which include both the existing unbalanced situation and the restricted access to verified data collections. The distribution of malignant images shows a significant underrepresentation when compared to the distribution of normal and benign pictures. Training mistakes impact the model's ability to detect substantial positive events when the instruction process becomes imbalanced. The research used data augmentation methods together with transfer learning techniques to solve these problems. Pre-trained models from natural image datasets establish transfer learning as a strong starting point which helps the process run faster while decreasing the need for extensive labeled medical data [19]. The combi-nation of transfer learning and SVMs has shown strong performance results even when using tiny datasets because deep features from transfer learning were applied [20]. The preliminary results showed positive outcomes yet most hybrid CNN-SVM systems designed for lung cancer detection failed to use advanced feature extraction methods and sophisticated hyperparameter tuning methods. The majority of research studies continue to use standard SVM settings while only conducting basic parameter testing which results in inadequate classification results [21]. The selection of CNN layers for feature extraction purposes remains an ongoing challenge. Features from shallow, intermediate, or deep layers encapsulate varying levels of abstraction, and their influence on final classification accuracy differs. The study aims to create a complete assessment of CNN layer selection together with SVM hyper parameter optimization to achieve better classification results. Our methodology targets superior accuracy results through the process of extracting distinctive features which we will feed into our precisely tuned SVM system [22]. We expect that this combination will achieve better results be-tween sensitivity and specificity when identifying malignant and benign lesions because these results are essential for making clinical decisions [23]. The study uses stratified sampling methods during cross-validation together with specific data augmentation techniques to ensure all classes which have low representation in the dataset receive proper representation. The research establishes a detailed repeatable process to classify lung cancer through its analysis of feature representation together with its methods for classifier development and dataset handling. The system demonstrates improved accuracy together with bet-ter interpretability which shows strong potential for use in medical workflows that support oncologists and radiologists with detecting diseases and creating customized treatment strategies [24].

### 1.1 Contributions of the Study

- A multimodal categorization system was created by the researchers. It includes deep convolutional feature extraction through VGG16 With the guidance of an SVM classifier to enhance lung cancer detection.
- The researchers used global average pooling to combine convolutional maps from multiple VGG16 network layers, which resulted in 512-dimensional embeddings that maintained both detailed and high-level morphological information.
- The researchers developed a complete patient database by combining histopathological image features with RNA-Seq transcriptomic data and clinical information and mass spectrometry proteomic data.
- We achieved multimodal fusion through the concatenation of normalized molecular data and clinical vectors with image embeddings because these two data types provided different patterns of spatial and biological and pathological information.
- By striking a balance between exploring and exploiting, the Dandelion Optimizer (DO) bio-inspired approach improves model performance and decreases the danger of achieving local optimums; as a consequence, it was used to optimize SVM hyperparameters.
- The team used Bayesian Optimization to improve their hyperparameter tuning process, which allowed them to search the entire space efficiently while developing a model that needed fewer evaluation tests to achieve better performance.
- The integrated framework demonstration established its superior performance over unimodal methods because it delivered reliable prediction results through its ability to analyze multiple patient data types.

## 2 Literature Review

Researchers in the area of deep learning have made a name for themselves by creating models that can improve the efficacy of diagnostic tests for lung cancer (LCa) and then using those models to classify cases [25],[26],[27]. This study delves into the SE-ResNeXt-50 model, which is enhanced with the use of Convolutional Neural Networks (CNNs). The SE-ResNeXt-50-CNN system incorporates its advanced features via its classification and ex-traction capabilities. The system employs dynamic quadri histogram equalization (QDHE) as its preprocessing method while applying methods for enhancing data and doing hyperparameter adjustment to boost its operational capabilities. Testing findings show that the system consistently performs well across several validation tests, establishing its strength with a 99.15% accuracy rate, 97.58% sensitivity rate, 99.51% precision rate, 99.80% specificity rate, and 98.54% F1-score [28]. Through the integration of machine learning (ML) methods with a multi-attribute decision-making strategy known as TOPSIS, lung X-ray pictures may be classified as either benign or malignant [29], [30]. The Inception v3 deep learning model serves as the evaluation tool to compare different classifiers for accurate classification purposes [31].

A thorough investigation into the detection and categorization of lung nodules was carried out by the researchers, who examined methods using deep learning and machine learning. Examining both classic ML techniques and state-of-the-art deep learning systems, the research aims to determine if ResNet-50 can im-prove classification accuracy [32].

The Improved Center Net framework shows major progress in the field because it solves previous model limitations through its use of ResNet-34 together with an attention mechanism which improves lung cancer detection accuracy [33]. The innovative method creates a lightweight vision transformer (LwViT) model which classifies lung cancer through analysis of CT images. We start by using Gaussian enclosed Bilateral Filtering (GaBF) to remove noise. Then, we use a conditional variational auto-encoder (CVA) for feature extraction. Lastly, we create an efficient deep learning system for classification by using a GroupWise Separable Convolutional dual attention-assisted Vision Transformer (gSC-DViT) [34]. The VGG16 CNN model is evaluated for its capacity to detect lung cancer in its initial stage and for its ability to predict disease progression. The method demonstrates an urgent requirement for medical diagnostic tools because lung cancer causes high rates of both sickness and death while deep learning methods will lead to better outcomes in early cancer detection and treatment procedures [35]. The study investigates how VGG16 and InceptionV3 and ResNet architectures per-form when assessed through model comparison tests which use annotated lung CT scans. The VGG model surpasses others in accuracy and inference speed, achieving higher sensitivity and specificity values [36]. A separate study examines hybrid deep learning models which combine Classifying lung lesions from CT scans using 1D-CNN-LSTM as well as VGG16-1D-LSTM architectures data. Among the three optimizers used by the models—AMAD, RMSprop, and SGD—the hybrid 1D-CNN-LSTM model yielded the best results when trained with Adam; this model attained 96% accuracy, 90% precision, 94.74% recall, and 92.31% F1-score [37]. Researchers have studied hybrid methods because they provide advantages in both efficiency and computation performance. In order to attain reduced computing demands while maintaining accurate classification findings, the researchers created an experimental setup consisting of a Feed-Forward Back Propagation Neural Net-work using a Support Vector Machine (SVM) [38].

A hybrid PSO-GA-SVM classification algorithm is used in the study, using the Cipto Mangunkusumo Hospital dataset located in Jakarta. Results compared to unoptimized SVMs are better when the Particle Swarm Optimization-Genetic Algorithm (PSO-GA) optimizes the parameters of support vector machines (SVMs) [39]. We develop a hybrid model that combines CNN and SVM, which can automatically classify lung images to detect the presence of cancer cells. This method demonstrates that CNNs require less training effort and have reduced parameter needs when compared to fully connected networks of similar scale while SVMs excel at eliminating nonessential data that harms their ability to classify information [40]. When data is scarce, the study use Principal Component Analysis (PCA) to get accurate classifications. PCA serves the purpose of reducing the number of features while maintaining essential information, and SVMs have shown better results than other classification techniques when used in these limited data situations [41].

**Table 1.** Recent Studies for Lung Cancer Classification

| Model / Approach | Dataset | Key Contributions | Limitations | Study |
|---|---|---|---|---|
| CNN + SVD + Ensemble (Voting) + ML classifiers | CT scan dataset (public) | High accuracy (99.49%), dimensionality reduction via SVD, explainability using Grad-CAM | High complexity, possible overfitting due to very high accuracy | [46] |
| CNN–SVM (OCNN-SVM) | Lung X-ray images | Combines CNN feature extraction with SVM classification, improved classification performance | Limited dataset, lacks multimodal integration | [13] |
| Neural Network + SVM (HNSVA) | Clinical + patient data | Reduces false negatives, improved prediction using hybrid learning | Higher computational cost, not image-focused | [47] |
| AlexNet + handcrafted features + mRMR + SVM/RF + SSA-GWO | Medical imaging dataset | Combines deep + radiomic features, optimized feature selection, improved accuracy | Complex pipeline, higher computational overhead | [48] |
| Multi-CNN (VGG19, ResNet, EfficientNet) + PCA + SVM | Histopathology images | Feature fusion, handles class imbalance, achieves near-perfect accuracy (99.9%) | Risk of overfitting, heavy computation | [49] |
| CNN–SVM | CT images | Simple hybrid model, improved accuracy (~97.9%), efficient classification | Limited feature diversity, no optimization techniques | [40] |
| CNN + Swin Transformer (C-Swin) | IQ-OTH/NCCD dataset | Combines local + global feature extraction, improved accuracy (96.26%) | Requires large computational resources | [50] |
| Optimized CNN (non-hybrid but efficient) | IQ-OTH/NCCD dataset | Lightweight, clinically deployable, high efficiency (94%) | No hybrid ML integration | [51] |
| CNN + Transformer (LungMaxViT) | Chest X-ray datasets | Explainable AI (Grad-CAM), strong generalization, high AUC | Not specific to lung cancer only | [52] |
| Hybrid AI (GLCM + SIFT + CNN) | IQ-OTH/NCCD dataset | Combines handcrafted + deep features, improved classification performance | Complex feature fusion, may increase processing time | [53] |

Lung cancer classification and segmentation are examined using the K-Nearest Neighbour (KNN), Support Vector Machine (SVM), as well as Data Structure (DS) approaches. The classification process uses lineament vectors which are derived from speech-extracted features of a metameric dataset. KNN together with post-processing techniques functions to improve region classification while enhancing segmentation accuracy [42]. With the use of computed tomography (CT) images, the suggested hybrid CNN-SVM architecture can classify lung cancer according to its stage and identify its various forms. The research demonstrates that hybrid systems improve diagnostic precision because they combine CNNs' ability to extract spatial features with SVMs' ability to classify data [43],[44],[45]. Table 1 offers a brief review of some recent works on the classification of lung cancer, focusing on different deep learning methods and

hybrid models. It offers an organized presentation of their datasets, significant findings, and drawbacks.

## 2.1 Research Gap

Existing research on lung cancer classification using deep learning and hybrid CNN-SVM techniques has shown encouraging results, but some significant gaps and restrictions remain un-addressed. Many previous research have relied on deep architectures like ResNet, DenseNet, and GoogLeNet, which, although strong, were initially built for large-scale natural picture datasets and may not perform well on relatively tiny and high-dimensional biomedical datasets. Their complex residual and inception-based structures prioritize high-level semantic representations and may fail to preserve fine-grained textural and morphological features required for accurate lung cancer analysis, whereas simpler models like AlexNet lack the depth required to learn rich hierarchical representations for complex medical image classification tasks. Furthermore, most previous studies have been conducted in a single-modality or single-dataset setting, frequently using only histopathological images, CT scans, or one type of omics data, limiting their ability to capture the heterogeneous nature of lung cancer as determined by tissue morphology, gene expression, protein abundance, and clinical characteristics. As a consequence, these unimodal techniques give only partial patient-level representations and exclude additional biological information that might in-crease classification robustness and accuracy. Furthermore, many current models use CNNs in an end-to-end way, with feature extraction and classification closely linked via fully connected layers, raising the danger of overfitting in restricted data settings. Hybrid CNN-SVM models have been introduced to reduce this problem. However, many of them rely on default or weakly optimized SVM parameters and do not adequately tune critical hyperparameters such as the regularization parameter (C) and kernel coefficient ($\gamma$), limiting their ability to form optimal nonlinear decision boundaries. Another significant limitation is the high hyperparameter tuning complexity of end-to-end deep learning frameworks like ResNet, DenseNet, and GoogLeNet, which typically necessitate extensive adjustments to learning rate, batch size, optimizer settings, regularization, and layer-wise fine-tuning, increasing computational cost and reducing reproducibility. To overcome these short-comings, this research suggests a new Dandelion optimizer-based hybrid VGG16-SVM architecture for multimodal lung cancer classification. VGG16 was chosen because it's simple and uniform convolutional architecture is more effective at preserving local spatial information and extracting fine-grained cellular and tissue patterns than AlexNet and provides sufficient representational depth compared to ResNet, DenseNet, and GoogLeNet. The incorporation of SVM improves generalization and reduces overfitting in high-dimensional feature spaces, especially for small biomedical datasets, while the Dandelion Optimizer efficiently tunes the most important SVM hyperparameters by balancing exploration and exploitation, resulting in faster convergence and improved classification performance with less tuning complexity. Most importantly, unlike previous studies that relied on a single dataset or modality,

the proposed framework is intended for a structured multimodal setting in which histopathological image features are integrated with transcriptomic, proteomic, and clinical data, allowing for a more comprehensive representation of lung cancer heterogeneity and thus improving robustness, accuracy, and clinical reliability.

# 3 Background Study

## 3.1 VGG 16

The architecture of VGG16 used for deep feature extraction is illustrated in Fig. 1 CNNs, or convolutional neural networks provide the basis of the VGG-16 model's design. With sixteen layers—eleven convolutional, three fully linked, and one Soft-max classifier—VGG is renowned for its depth. "Very Deep Convolutional Network for Large Scale Image Recognition," a 2014 study by Karen Simonyan and Andrew Zisserman, introduced the VGG-16 architecture. Using both convolutional and fully linked layers, Karen and Andrew built a 16-layer network. In order to simplify matters, a sequence of 3×3 convolutional layers will be used [54]. Each of the two convolutional layers, the first and second, has 64 feature kernel filters that are 3×3 dimensional. By the time the input RGB image has made it the size has varied from 3x3 to 224x224x64 across the first two convolutional layers. The output is then sent to the maximum pooling layer via a two-step stride. Two feature kernel filters with a size of three by three make up the third and fourth convolutional layers. Following the separation of the two layers by a max pooling layer with a stride of 2, the output is reduced to 56x56x128. The convolutional layers that follow have kernel sizes of 3x3. Every one of them makes use of 256 feature maps. After that comes a two-step maximum pooling layer. The two sets each include eight to thirteen convolutional layers with a 3×3 kernel size. The convolutional layers of each set include 512 kernel filters. These layers are followed by the 1-stride max-pooling layer.

After a 1000-unit SoftMax output layer, there are two tiers of 4096-unit totally connected hidden layers. Developing a visual representation of vast collection of annotated pictures. Using ImageNet, several pretrained models have received instruction, including Inception V1, Inception V2, VGG-16, and VGG-19, despite the network's large picture variation. Extensive training of these custom-built models is done utilizing GPUs on massive datasets containing hundreds of picture categories and millions of photos. The model's extensive training on a huge dataset gives it a firm grip on low-level variables, including forms, illumination, rotation, edges, and spatial relationships. You may use these features to help with knowledge transfer and feature extraction in computer vision challenges [55]. Fig.1. shows VGG 16 Architecture below.


**Fig. 1.** VGG 16 Architecture

Convolutional layers:

$$A_i = \sigma(W_i * A_{i-1} + b_i), \text{"for "} i = 1,2, \ldots, n \quad (1)$$

Where:

- $A_i$: is the output feature map of the $i^{th}$ layer.
- $A_{(i-1)}$: Input to the $i^{th}$ layer; for the first layer, this is the input image I.
- $Wi$: Learnable convolutional filter weights of the $i^{th}$ layer.
- $b_i$: adds a bias term to the convolution.
- *: Convolution operation.
- σ: Activation function, typically ReLU (Rectified Linear Unit).

This equation represents how features are learned by convolving the input with filters, adding a bias, and applying a non-linear activation.

**Pooling layers:**
Pooling procedures decrease spatial after convolutional layers dimensions while keeping the most important details intact. The pooling operation (commonly max pooling) is given by:

$$P_i = P(A_i), \text{ for selected layers} \quad (2)$$

- *Pi*: Output of the pooling operation at layer ith.
- *Ai*: feature map that was input by the prior convolutional layer.
- *P*: The pooling function, often known as max pooling, chooses the highest value in a certain area.

Pooling helps reduce computation, control overfitting, and retain translation invariance.

**Feature vector:**

To prepare the output for passing to a classifier, it is necessary to flatten it after the final pooling layer:

$$F=\text{Flatten}(P_n) \tag{3}$$

- $F$: Feature vector derived from the CNN.
- $P_n$: Final pooling layer output.
-

The process of flattening transforms multidimensional tensor data into a vector format that classification systems can use which includes fully connected layers and external classifiers such as SVM.

### 3.2 Support Vector Machine (SVM)

Fig. 2. shows the full SVM classifier system that was used for this investigation. One kind of supervised learning technique that seeks to determine the optimal hyper-plane is support vector ma-chines, or SVMs that will separate input data points into different classes [56]. The optimization issue is expressed as for a dataset that can be separated along linear lines:

$$\min_{w,b} \quad \frac{1}{2} \| w \|^2 \tag{4}$$

subject to:

$$'y_i(w \cdot x_i + b) \geq 1, \forall i' \tag{5}$$

- $w$: The hyperplane's weight vector.
- $b$: Bias term.
- $xi$: Feature vector of the $i^{th}$ sample.
- $yi \in \{-1, 1\}$: Class label of the $i^{th}$ sample.

The constraint guarantees that all samples are classified correctly with a margin of at least 1.

While achieving a lower perplexity and a higher burstiness, the goal of this formulation is to close the space between classes. The SVM system uses kernel functions to process data that cannot be linearly separated using the kernel function K(xi, xj) which enables the system to create higher-dimensional spaces that permit linear data separation. RBF, linear, and polynomial functions rep-resent the most commonly used kernel types. The optimization problem exists in two different representations: one uses Lagrange multipliers and the second one uses this alternate form:

$$'maximize \quad \sum_i \alpha_i - \tfrac{1}{2}\sum_i\sum_j \alpha_i\alpha_j y_i y_j K(x_i, x_j)' \tag{6}$$

$$subject\ to \quad 0 \leq \alpha_i \leq C, and \quad \sum_i \alpha_i y_i = 0 \tag{7}$$

- $\alpha_i$: Lagrange multipliers.
- C: An individual's ability to manage the compromise between margin size and misclassification.

- K(xi, xj): Kernel function (e.g., linear, polynomial, RBF).
- The optimization which solves this problem results in the optimal decision boundaries in the transformed space.

This formulation gives SVM flexibility in managing high-dimensional data more efficiently, thereby making it suitable for anomaly detection tasks [57].

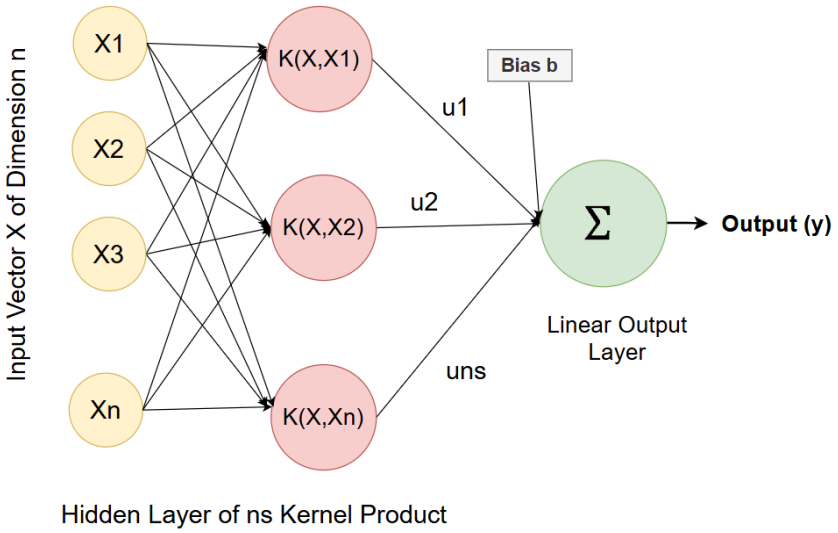


**Fig. 2.** Support Vector Machines (SVM) Architecture.

### 3.3 Dandelion Optimizing Algorithm

DO program, inspired by biology, makes a working of a technology similar to the wind-powered movements of a dandelion seed. It consists of three phases: ascension, fall, and landing [58]. During the ascension phase, seeds spread across a community by air circulation or spiral upwards. During the falling and landing phases, flying seeds alter their path using L´evy random walks and Brownian motion rules. The DO algorithm employs an evolutionary technique, offering the benefit of easy processing. The self-adaptive feature improves convergence to local minima, while a memory-based approach prevents premature con-vergence. Unlike other metaheuristic algorithms, the DO may find the optimal global solution by considering the whole population. The mathematical model for DO is shown below.

$$\text{population} = \begin{bmatrix} x_1^1 & \cdots & x_{\text{dim}}^1 \\ \vdots & \ddots & \vdots \\ x_1^N & \cdots & x_{\text{dim}}^N \end{bmatrix} \tag{8}$$

The number of variables in the problem and the number of seeds in the swarm are indicated by this matrix, N× dim . Stage one involves applicant roles

$$\text{lb} = [lb_1, \ldots, lb_{\text{dim}}] \tag{9}$$

are randomly picked from the problem's lower limits and

$$\text{ub} = [ub_1, \ldots, ub_{\text{dim}}] \tag{10}$$

from the upper limits, and the individual $x_i$ is modelled by the equation below.

$$x_i = lb + \text{rand} \times (ub - lb) \tag{21}$$

According to Eq. (12), $x_{\text{elite}}$the procedure begins with the individual who has the greatest fitness value. The following equation describes it:

$$x_{\text{elite}} = \min\ f(x_i) \tag{32}$$

$$x_{\text{elite}} = x_i \quad \text{such that} \quad f_{\text{best}} = f(x_i) \tag{43}$$

During the exploration phase of the method, seeds are dispersed based on wind height and speed (Y) along their axis [59]. Throughout the process, the turbulence surrounding the seeds is updated to create a continuous upward spiral, as seen in the equations below.

$$x^{t+1} = x^t + \alpha \times v_x \times v_y \times \ln(Y) \times (x^t - x_s) \tag{54}$$

$$x_s = \text{rand}(1,\text{dim}) \times (ub - lb) + lb \tag{65}$$

# 4 Methodology

This research suggests a multimodal lung cancer categorization system that includes histopathological pictures, transcriptomic-clinical profiles, and proteomic data. The approach consists of six stages: (i) data collection, (ii) modality-specific preprocessing, (iii) feature extraction, (iv) multi-modal feature fusion, (v) hybrid classification with optimization, and (vi) assessment. The original framework combines a VGG16 deep learning feature extractor with a classifier that uses Support Vector Machines (SVMs) which uses Dandelion Optimizer (DO) for its hyperparameter tuning.

## 4.1 Data Collection

The research study develops a multimodal classification system for lung cancer by combining three distinct data types which include histological images and transcriptomic profiles with clinical metadata and mass spectrometry-derived proteomic data. The three datasets deliver distinct biological information which together enhance diagnostic precision and enable advanced feature development.

**LungHist700 – Histological Image Repository**

The LungHist700 collection received 691 high-resolution histological images which 45 patients who had pulmonary tissue surgery at Hospital Cl´ınico Universitario de Valladolid provided in 2023. Histological images consist of stained tissue sections which scientists analyze under a micro-scope to study cell structures and disease-related changes. The dataset features samples from healthy tissue found in the lungs as well as

NSCLC which makes it appropriate for binary classification the tissues that are malignant and those that are not. The CEIm A´rea de Salud Valladolid Este approved the project after obtaining ethical consent (Project ID: PI 23-3167).
**Data Source link**: LungHist700 Dataset on Figshare. Data Source link: Proteomic Data Commons (PDC).

### 4.2 Data Description

For this study, three data modalities enable a rich and detailed portrayal of lung cancer at the cellular, molecular, and proteomic levels:

The dataset contains 691 JPEG images which show lung tissue samples from both nor-mal patients and NSCLC patients. The resolution of the images stands at 1200x1600 pixels while the im-ages show details at 20x and 40x magnification. The subtypes of adenocarcinoma specimens include different training methods which improve model generalization while solving the problem of class imbalance. The Albumentations library provided medical imaging applications with effective augmentation capabilities which included random rotations between 0° and 360°, horizontal and vertical flips, and zoom transformations between ±10% and color jittering with brightness/contrast adjustments of ±15% [60]. The training set received 80% of patients and their corresponding patches, such that no patient-specific information leaked, while the rest was split evenly across the validation and testing groups. One-hot vectors were used for CNN training, while SVM classification employed integer labels as their training method. The dataset originated with 691 images and grew to 3,103 images after the process of augmentation.

**Preprocessing of Gene Expression and Clinical Data (TCGA LUAD 2016)** The research used RNA-Seq gene expression data which contains log-transformed transcripts per million (TPM) data that researchers collected and filtered to keep only the most variable genes through variance thresholding. The study removed genes that showed less than 20% variance across samples to reduce noise and improve distinguishing power. The expression values were subsequently z-score normalized across all patients to standardize the scale. The researchers analyzed clinical metadata which included age information and gender information and smoking status information and tumor stage information as separate data points. The study used one-hot encoding to transform categorical attributes which included gender with its two sex, smoking status (smoker or non-smoker), and other variables. The researchers combined the purified gene expression data with the clinical data to create a single structured feature vector which represented each patient. The study maintained only those patients who had complete information for every required field as this approach ensured consistent data for fusion process.

**Proteomic Data Preprocessing (PDC000219 – LUAD100 Proteome)**
The processed protein abundance matrix from the CPTAC proteomic dataset (PDC000219) was utilized. The study excluded proteins which had more than 20% missing data across all samples. The outstanding K-nearest neighbors (KNN) imputation was used to fill in missing variables. The protein abundance values were log2-

transformed and z-score normalized across samples to achieve uniform scaling. Samples were filtered to include only those associated with patients possessing valid clinical annotations and cancer status labels (LUAD versus normal). These labels were subsequently utilized for binary classification. In instances of duplicate protein entries caused by isoforms, mean aggregation was employed to consolidate the values.

### 4.3 Feature Extraction

Following preprocessing, modality-specific feature extraction was performed to generate structured numerical representations for each patient. For histopathology pictures, the convolutional basis of the pre-trained VGG16 network was used. The images were divided into separate 224 × 224 patches which did not overlap while Global Average Pooling was used to extract feature maps from convolutional layers. Patch-level characteristics were averaged to provide a patient-level histological description (Hi). The study used variance filtering to retain informative genes from transcriptomic-clinical data while using one-hot encoding for categorical clinical variables and scaling continuous attributes to the range of [0,1]. The analyzed data was concatenated into a transcriptomic-clinical vector (Ti).

**TCGA LUAD 2016 – Gene Expression and Clinical Metadata**

The TCGA LUAD 2016 dataset was obtained from the Lung Cancer Explorer platform which contains RNA-Seq-based gene expression data for lung adenocarcinoma (LUAD) patients together with their clinical information that includes age, sex, smoking status, survival duration, and pathological staging details. The dataset enables researchers to extract features from both molecular data which includes gene expression and demographic data to improve patient classification and enable supervised learning activities.

**PDC000219 – Academia Sinica LUAD100 Proteome Dataset**

This dataset comprises mass spectrometry-derived proteomic data from LUAD and normal tissue samples, provided by the Academia Sinica research group as part of the CPTAC program. It offers downstream protein expression data obtained from tandem mass tag (TMT10)-labeled quantification. This study utilizes the processed protein abundance matrix for classification, despite the avail-ability of raw spectral (RAW) files. Clinical annotations are accessible for the designation of cancer status and degrees of differentiation. These data are appropriate for patch-based analysis and convolutional feature extraction. This dataset comprises mass spectrometry-derived proteomic data from LUAD and normal tissue samples, provided by the Academia Sinica research group as part of the CPTAC program. It offers downstream protein expression data obtained from tandem mass tag (TMT10)-labeled quantification. This study utilizes the processed protein abundance matrix for classification, despite the availability of raw spectral (RAW) files. Clinical annotations are accessible for the designation of cancer status and degrees of differentiation. These data are appropriate for patch-based analysis and convolutional feature extraction.

**Transcriptomic and Clinical Data (TCGA LUAD 2016)**

The RNA-Seq data comprises normalized gene expression values for more than 20,000 genes from numerous LUAD patients. The study records clinical data which includes

patient sex, patient age, tumor stage, smoking history, and survival outcomes. The method enables researchers to extract transcriptomic data which they can use to study the relationship between phenotypic traits and demographic characteristics.

**Proteomic Data (PDC000219—LUAD100 Proteome)**

The dataset provides mass spectrometry-based protein abundance data which coVers

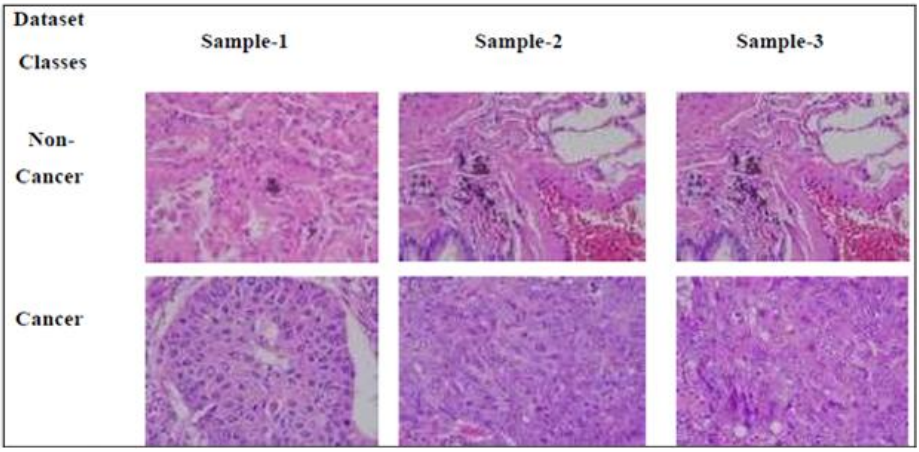


**Fig. 3.** Representative histopathological image samples

more than 6000 proteins found in LUAD and normal tissue samples. The TMT10 multiplexing method was used to conduct protein quantification and the resulting abundance matrices can be accessed in TSV format. The features show biological functions which depend on their functions and they serve as fundamental elements for biological systems. Fig. 3. shows Representative histopathological images samples.

### 4.4 Data Preprocessing

To maintain consistency across different data types we developed specific preprocessing pipelines which prepared the datasets for multimodal integration and classification. The procedures include stain normalization for histological images and normalization and filtration of transcriptomic and clinical data and standardization of proteomic profiles. After processing each modality through its dedicated preprocessing steps all features were transformed into a standard format which enabled their use in upcoming fusion and classification processes.

**Preprocessing of Histological Images (LungHist700)**

The LungHist700 images were processed to conform to the VGG16 architecture and normalized utilizing the Macenko technique with the Slide flow library. The inter-sample color variability was reduced because different H&E staining methods and scanner settings caused color differences between samples [61]. The researchers used non-overlapping image divisions with 224 × 224-pixel dimensions for image processing after they completed normalization. Otsu's thresholding was used to convert images into

greyscale, which resulted in the removal of patches that contained less than 80% tissue because these patches showed dominant background elements.

The Keras preprocess input function for VGG16 scales pixel values to the [0, 1] range while normalizing each channel through mean subtraction and standard deviation division using ImageNet dataset statistics [62]. The researchers implemented dynamic data augmentation methods. The researchers performed missing data imputation for proteomic data while they transformed abundance values through log2-transformation and z-score normalization. The resulting profiles generated a structured proteome vector which represented the data (Pi).

To facilitate effective multimodal learning, the extracted feature vectors from each modality—histopathological features derived from VGG16, transcriptomic-clinical features, and proteomic features—were aligned at the patient level. To make sure that the integration was consistent, only samples with complete multimodal information were kept. After that, these representations for each modality were put together into a single feature space so that they could be used for classification later on.

### 4.5 Multi Modal Feature Fusion

The procedure generated three distinct feature representations for each modality, denoted as histopathological features (H_i ), transcriptomic-clinical features (T_i ), and proteomic features (P_i ), which were ready for integration across many modes.

In order to effectively merge data from several sources, a feature-level fusion (early fusion) approach was used. In this method, modality-specific feature vectors for the same patient were first aligned at the patient level. This made sure that each sample had consistent multimodal information. Unified fusion was only done for patients who had all of their data from all modalities.

Before fusion, all feature vectors were normalized and scaled to a common range to make sure they were compatible and to stop one modality from taking over the learning process. When combining several forms of data, such as picture features and omics data, this phase is crucial.

The characteristics that were retrieved were integrated into one representation so that the strengths of each modality could be used. A multimodal feature vector is defined as follows for every patient i:

$$\mathbf{F}_i = [\mathbf{H}_i, \mathbf{T}_i, \mathbf{P}_i] \tag{76}$$

where $F_i$ represents the fused multimodal feature vector for patient i, obtained through feature concatenation of modality-specific representations.

This type of fusion, which is based on concatenation, makes it possible to combine complementary biological information. For example, histological features show how tissues look, transcriptomic-clinical features show how genes are expressed and patient metadata, and proteomic features show how proteins work. The model's ability to shed light on complex nonlinear interactions as well as biological variability in lung cancer is enhanced by this unified depiction. This integration guarantees that morphological patterns derived from histology, molecular signals obtained from transcriptomics and

clinical data, and proteomic expression profiles collectively enhance precise cancer classification.

In instances when one or more modalities were absent, a late- fusion method was used. Separate training was done for independent classifiers on the available modalities, and their prediction probabilities were pooled using weighted averaging:

$$P(y_i = 1) = \alpha_1 P_H + \alpha_2 P_T + \alpha_3 P_P \tag{87}$$

subject to:

$$\alpha_1 + \alpha_2 + \alpha_3 = 1, \alpha_k \geq 0 \tag{98}$$

In this case, $P_H$, $P_T$, and $P_P$ are the predictions from the histological, transcriptomic–clinical, and proteomic classifiers, respectively. The fusion weights (α1, α2, α3) were adjusted on the validation set to provide the most confidence.

To ensure compatibility between modalities, all final vectors were standardized to a common scale. Where dimensional incompatibilities occurred. The feature dimensions were harmonized using Principal Component Analysis (PCA) or zero-padding, resulting in a unified dataset suitable for hybrid classification.

### 4.6 Model Building

Following multimodal feature fusion, the unified patient-level feature vectors Fi = [Hi, Ti, Pi] were fed into a hybrid classification framework that combines classifier that uses hyperparameter-ter tweaking and a Support Vector Machine (SVM) the Dandelion Optimizer. This architecture guarantees that the discriminative power of deep features (VGG16-based) is preserved in the dimensional space.

To represent the complicated, nonlinear patterns in multimodal lung cancer data, the RBF kernel, standing for Radial Basis Function was used.

$$'K(\mathbf{F}i, \mathbf{F}j) = \exp - \gamma \| \mathbf{F}i - \mathbf{F}j \|^2 , \tag{109}$$

where γ determines the influence of individual training samples on the decision boundary. The RBF kernel was selected due to its effectiveness in modelling nonlinear relationships in high-dimensional biological data.

For the suggested hybrid framework to operate, finding the best SVM hyperparameters that maximize classification performance while ensuring generalization across unseen data. This is formulated as the following optimization problem:

$$\max_{C,\gamma} \; J(C,\gamma) = \frac{1}{K} \sum_{k=1}^{K} \text{Accuracy}_k \tag{20}$$

where J(C,γ) signifies the goal function,

which is characterized as the mean classification accuracy over K-fold cross-validation, and C and γ are the SVM regularization and kernel parameters. Accuracy is used as the main optimization measure because it is stable and easy to understand in balanced classification situations. For a comprehensive evaluation, other measures are used, such as recall, accuracy, precision, and area under the curve (AUC).

The Dandelion Optimizer (DO) serves as the fundamental tool for precise hyperparameter tuning. To achieve a balance between global exploration and local exploitation inside the search space, it mimics the seed distribution as well as adaptive survival behavior of dandelion plants. The 5-fold cross-validation accuracy on the set of validations is used to evaluate the fitness of the candidate solutions (C,γ). DO efficiently converges toward optimum hyperparameter configurations via iterative updates, circumventing local optima, thereby rendering it suited for high-dimensional optimization problems.

The final hybrid framework combines deep representations extracted from the VGG16 convolutional neural network so it uses characteristics derived from the most recent completely linked layer and SVM's non-linear classification abilities through its RBF kernel and the hyperparameter optimization from DO. This system produces a multimodal lung cancer classification system which achieves better diagnostic accuracy through its generalizable capabilities.

### 4.7 Objective Function

The Dandelion Optimizer is used to maximize the classifier's validation performance in order to identify the ideal SVM hyperparameters. Since cross-validation is not used in the model, the following definition of the objective function is based on validation accuracy:

$$\max_{C,\gamma} \mathcal{J}(C,\gamma) = \text{Acc val}\ (C,\gamma) \tag{21}$$

where C is the SVM regularization parameter, γ is the RBF kernel coefficient, and Accval (C,γ) denotes the classification accuracy obtained on the validation set for a given pair of hyperparameters. The optimizer searches for the values of C and γ that yield the highest validation accuracy. Consequently, the ideal collection of hyperparameters is provided by

$$(C^*\gamma^*) = arg\ max\ J(C,\gamma) \tag{22}$$

Use this instead if you want a slightly stronger version to avoid overfitting:

$$\max_{C,\gamma} J(C,\gamma) = ACC_{val}(C,\gamma) - \lambda \mid Acc_{train}(C,\gamma) - Acc_{val}(C,\gamma) \mid \tag{23}$$

enhances validation accuracy while imposing penalties for significant discrepancies between training and validation performance, thereby promoting superior generalization.

**Table 2.** Hyperparameter Tuning Complexity Comparison of CNN Models.

| Model | Depth | No. of Tunable Hyperparameters | Tuning Complexity (1–5) | Overfitting Risk (1–5) |
|---|---|---|---|---|
| AlexNet | 8 | 6–8 | 2 | 3 |
| GoogLeNet | 22 | 10–14 | 4 | 4 |
| ResNet-50 | 50 | 12–18 | 5 | 4 |
| DenseNet121 | 121 | 14–20 | 5 | 4 |
| **VGG16 (Selected)** | 16 | 5–7 | **2** | **2** |

In comparison to alternative designs form Table-2, VGG16 offers the best mix between representational power and computational simplicity, which is why it is chosen as the feature extraction model. Deeper models, like ResNet-50 and DenseNet121, need a much larger number of adjustable hyperparameters, as table illustrates. This leads to increased tuning complexity and an increased danger of overfitting, especially in small and high-dimensional biomedical datasets. GoogLeNet's intricate inception design makes optimisation more challenging even as it captures multi-scale information. Conversely, AlexNet is less complicated, but it is not deep enough to understand the specific and distinguishing characteristics needed for lung cancer analysis. VGG16, on the other hand, provides intermediate depth with a straightforward and consistent convolutional structure, allowing for the efficient extraction of fine-grained features while preserving less overfitting risk and tuning complexity. Table 3 shows CNN model Comparison

**Table 3.** Hyperparameter Tuning Complexity Comparison of CNN Models.

| Parameter | Description | Type | GridSearchCV Range | Bayesian Optimization Range |
|---|---|---|---|---|
| C | Regularization parameter controlling margin softness | Continuous | {0.1, 1, 10, 100} | $[0.5{\cdot}C^*, 1.5{\cdot}C^*]$ |
| Kernel | Kernel function used in the SVM | Categorical | {linear, rbf} | Fixedfrom GridSearch |
| $\gamma$ | RBF kernel coefficient (RBF kernel only) | Continuous | {scale, auto,0.001,0.01,0.1,1} | $[0.1 \cdot \gamma^*, 10 \cdot \gamma^*]$ |
| CV | Number of cross-validation folds | Integer | 5 | 5 |
| Scoring | Evaluation metric | Categorical | {accuracy, f1} | Same as GridSearchCV |
| Search method | Search strategy | Categorical | Exhaustive (GridSearchCV) | Bayesian optimization |

### 4.8 Performance Metrics

Accuracy: One of the two simplest ways to measure the easily observable percentage of times the classifier makes correct predictions is accuracy. The proportion of correctly predicted positive outcomes relative to the total number of forecasts is one way to look at it. Precisely, precision is characterized as:

$$\text{Accuracy} = \frac{TP+TN}{TP+TN+FP+FN} \tag{24}$$

Where,

- 'TP=True Positives
- TN= True Negatives
- FP= False Positives
- FN= False Negatives'

Precision: The majority of positive cases are properly identified using precision measurements. What determines this is:

$$'\text{Precision} = \frac{TP}{TP+FP}' \tag{25}$$

Recall A detection system's sensitivity, also known as recall, is the percentage of correctly detected true positives by the classifier:

$$'\text{Recall} = \frac{TP}{TP+FN}' \tag{26}$$

F1-Score the F1-score is a harmonic mean of the recall and accuracy:

$$'F_1 = \frac{2*Pr\,ecision*Re\,call}{Pr\,ecision+Re\,call}' \tag{27}$$

Algorithm 1: Hybrid VGG16 + SVM Multimodal Lung Cancer Classification Framework

Require: Histology images I, Transcriptomic data T , Proteomic data P , Clin-ical metadata C
Ensure: Predicted class labels Y
1: // Histology Image Preprocessing
2: for each image i ∈ I do
3: Apply Macenko stain normalization
4: Extract non-overlapping 224 × 224 patches
5: Remove background-dominated patches
6: Apply data augmentation (flip, rotate, scale)
7: end for
8: // Feature Extraction using VGG16
9: for each preprocessed image patch do
10: Pass patch through pretrained VGG16 network
11: Aggregate multi-scale convolutional features
12: Apply global average pooling

13: Obtain 512-dimensional histology embedding H
14: end for
15: // Multimodal Data Integration
16: Normalize transcriptomic data T
17: Normalize proteomic data P
18: Normalize clinical metadata C
19: Concatenate H, T, P, and C to form fused patient-level feature vector F
20: // SVM Hyperparameter Optimization using Dandelion Opti-miser
21: Initialize population of candidate hyperparameters (C, γ)
22: Define objective function:
J(C, γ) = Accval(C, γ)
23: while termination criterion not met do
24: for each candidate solution (C, γ) do
25: Train SVM with RBF kernel on training data using (C, γ)
26: Evaluate validation accuracy Accval(C, γ) 27: Compute fitness: J (C, γ) = Accval(C, γ) 28: end for
29: Update candidate solutions using Dandelion optimizer
30: Retain the best candidate solution
31: end while
32: Select optimal hyperparameters:
(C∗, γ∗) = arg max J (C, γ)
33: // Final Training and Prediction
34: Train final SVM on fused feature vector F using (C∗, γ∗)
35: Predict class labels Y for test data
36: // Performance Evaluation
37: Compute Accuracy, Precision, Recall, F1-score, and AUC
38: Compare results with baseline and unimodal models

## 5 Results And Discussions

A comparison of how well each model, including the suggested Hybrid VGG16 + SVM and baseline networks, is presented in this research, which compares the proposed Hybrid VGG16 + SVM model optimized using the Dandelion optimizer (DO) against baseline models include ResNet-50, Dense-Net121, and a custom CNN. The assessment was carried out using multimodal data that included histopathological, transcriptomic-clinical, and proteomic aspects, with measures like recall, F1-score, accuracy, As well as area under the curve (AUC). The findings reveal that the DO-optimized hybrid model outperformed the unimodal and conventional baselines, as confirmed by conflicting information and ROC curves. Training, validation, as well as testing were all carried out using patient-level divisions to ensure data leakage was prevented.

Table 4 shows that when compared to the baseline models, the suggested DO-optimized Hybrid VGG16+SVM model performs much better. With an area under the curve (AUC) of 0.99 and an accuracy score of 0.9694, this model clearly excels in class distinction. Notably, the model has a recall rate of 0.9895, indicating that it successfully

identifies cancerous samples. The suggested model's performance differs by around 8-10% when compared to DenseNet121 and ResNet-50. the efficacy of integrating deep feature extraction with support vector machine (SVM)-based classifications and hyperparameter tweaking using the Dandelion optimizer) with respect to accuracy.

**Table 4.** Performance comparison of classification models

| ‘Model | Accuracy | Precision | Recall | F1-Score | AUC |
|---|---|---|---|---|---|
| Hybrid VGG16+SVM | 0.9694 | 0.9711 | 0.9895 | 0.9802 | 0.99 |
| DenseNet121 | 0.8790 | 0.9000 | 0.9470 | 0.9230 | 0.92 |
| ResNet-50 | 0.8650 | 0.8900 | 0.9390 | 0.9140 | 0.89 |
| CNN | 0.8116 | 0.8683 | 0.8884 | 0.8783 | 0.87’ |

**Table 5.** Performance comparison of classification models

| Model | Accu-racy | Preci-sion | Recall | F1-Score | AUC |
|---|---|---|---|---|---|
| Hybrid VGG16 + SVM (No Tuning) | 0.932 | 0.9405 | 0.962 | 0.9511 | 0.95 |
| DenseNet121 | 0.865 | 0.885 | 0.93 | 0.907 | 0.9 |
| ResNet-50 | 0.85 | 0.872 | 0.92 | 0.895 | 0.88 |
| CNN | 0.79 | 0.85 | 0.87 | 0.86 | 0.84 |

In order to evaluate the impact of optimizing the hyperparameters, Table 5 offers a comparison be-tween the results obtained from models where hyperparameter optimization is not done and the ones achieved via DO optimization process. This makes it possible to identify the effects of the DO on the improvement of the classifier. It is evident from this that optimizing the model's hyperparameters via DO significantly enhances its performance. For instance, the Hybrid VGG16+SVM without optimization has a classification accuracy of 0.9320 while after optimization, the classifier per-forms at 0.9694 accuracy.

### 5.1 Confusion Matrix

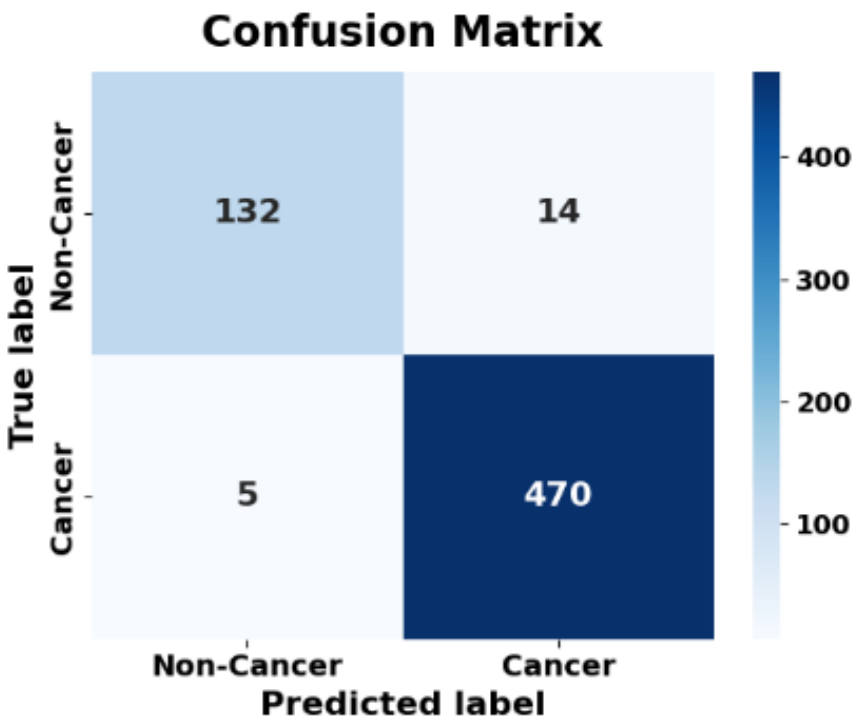


**Fig. 4.** Confusion matrix of Hybrid VGG16+ SVM.

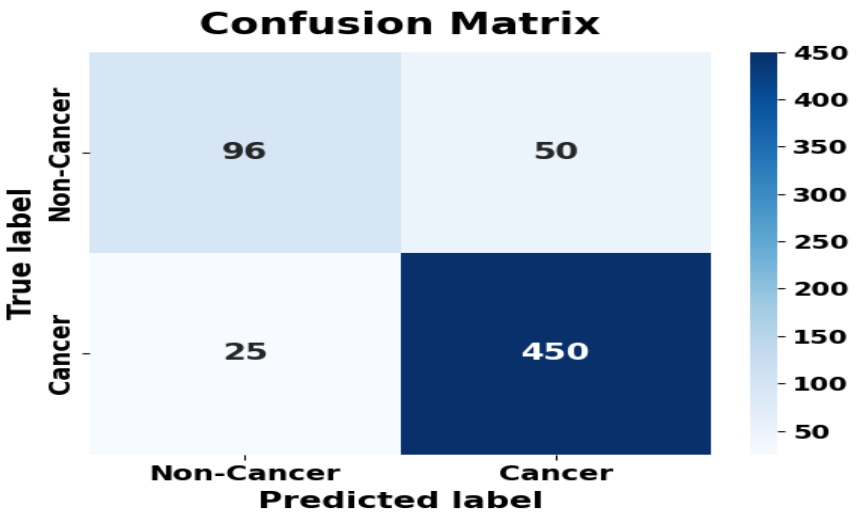


**Fig. 5.** Confusion Matrix of DenseNet121

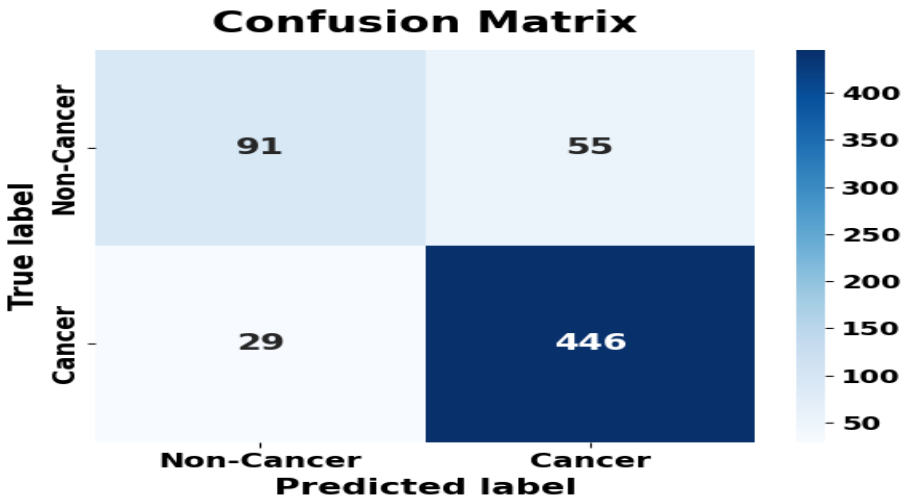


**Fig. 6.** Confusion matrix of ResNet-50

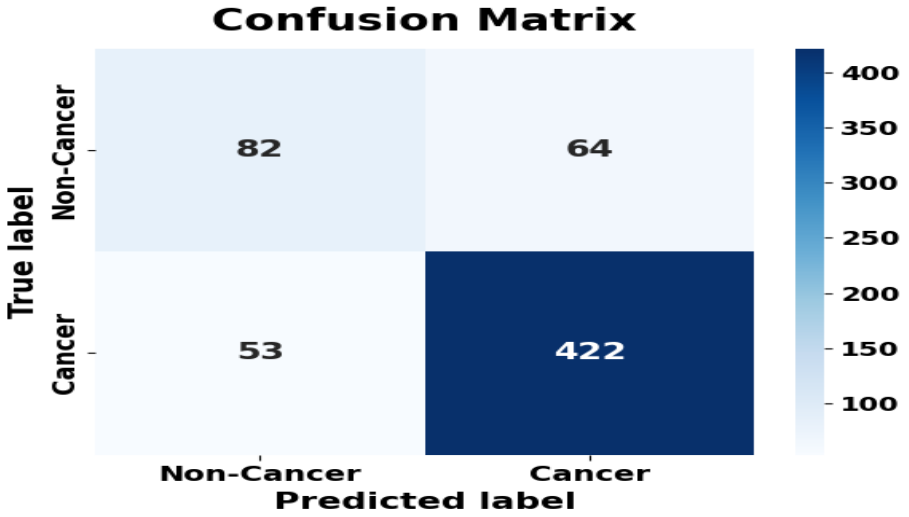


**Fig. 7.** Confusion matrix of custom CNN

The Hybrid VGG16 + SVM model present in Fig.4. shows its performance after Dandelion Optimizer (DO) optimization because it successfully identified 132 non-cancer samples while misidentifying only 14 healthy samples as malignant thus demonstrating a low false positive rate. The system achieved its objective by correctly diagnosing 470 cancer patients while making only 5 false negative mistakes which showed it maintained an effective balance between sensitivity and specificity. The model achieves su-

perior diagnostic results because it combines deep feature extraction with SVM classification and DO-based hyperparameter optimization which optimizes diagnostic performance through its adaptive exploration-exploitation balance method.

Fig.5. shows the confusion matrix for DenseNet121, which successfully detected 96 non-cancer cases but misidentified 50 healthy samples as malignant, increasing the false positive rate when compared to the suggested model. While 450 cancer cases were successfully identified, 25 malignancies were missed, showing a slight decrease in sensitivity and specificity. Fig. 6. shows Res-Net-50's performance, which accurately forecasted 91 non-cancer cases but misclassified 55, while recognizing 446 true positives and missing 29, indicating equal sensitivity to DenseNet121 but a larger propensity to overdiagnosis. Fig.7. displays the results of the bespoke CNN model, which accurately identified 82 non-cancer samples but produced 64 false positives, the most of any model. It correctly recognized 422 cancer patients but failed in 53, indicating the least favorable sensitivity and specificity. When it comes to classification accuracy, our research shows that the suggested Hybrid VGG16-SVM model with DO provides the optimal mix of sensitivity and specificity.

### 5.2 ROC Curve

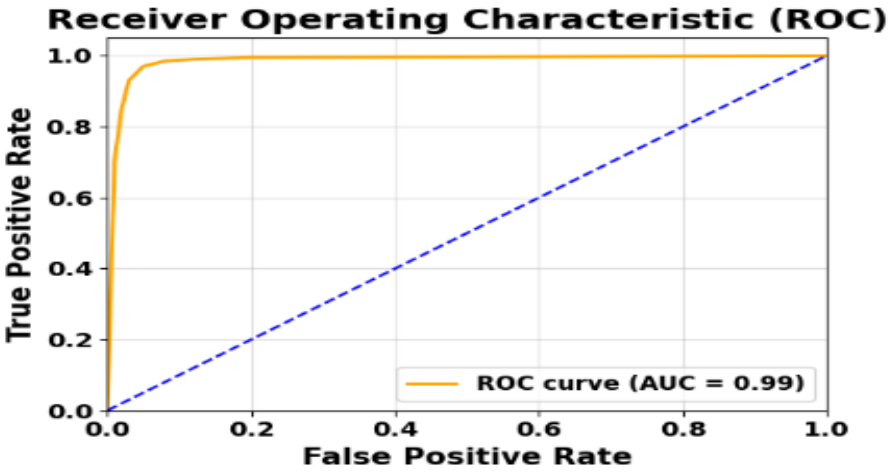


**Fig. 8 ROC curve of Hybrid VGG16 + SVM (DO-optimized)**.

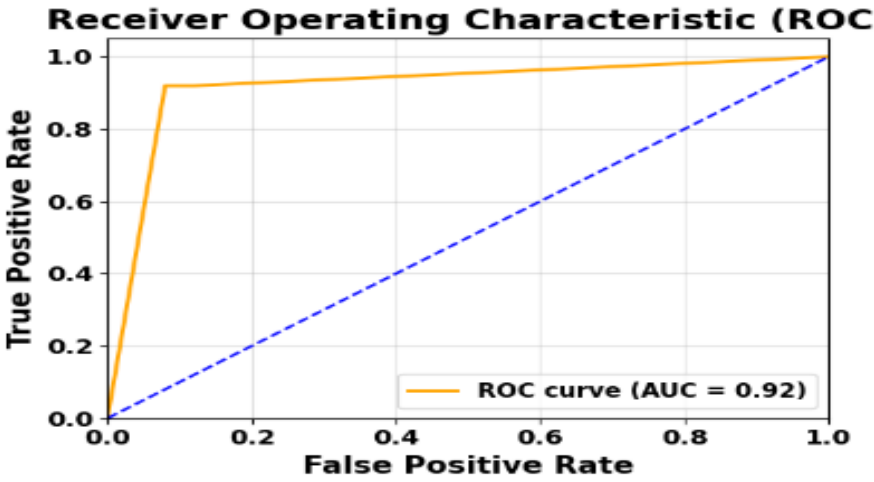


**Fig. 9 ROC curve of DenseNet121.**

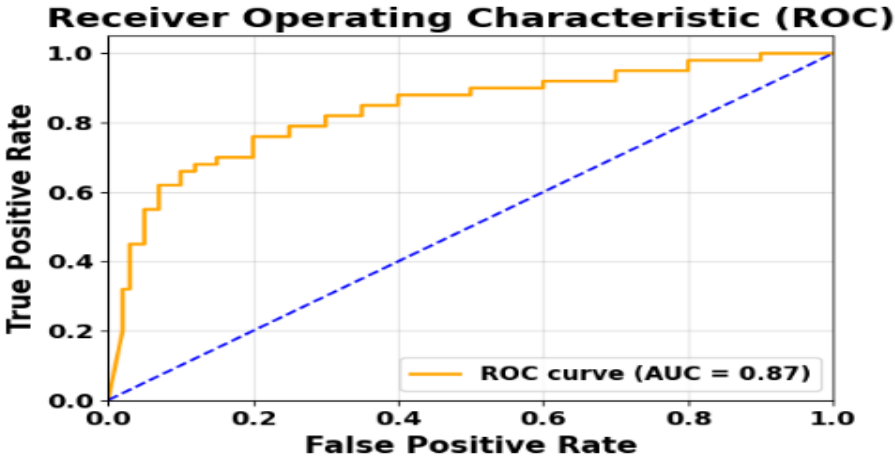


**Fig. 10 ROC curve of ResNet1-50.**

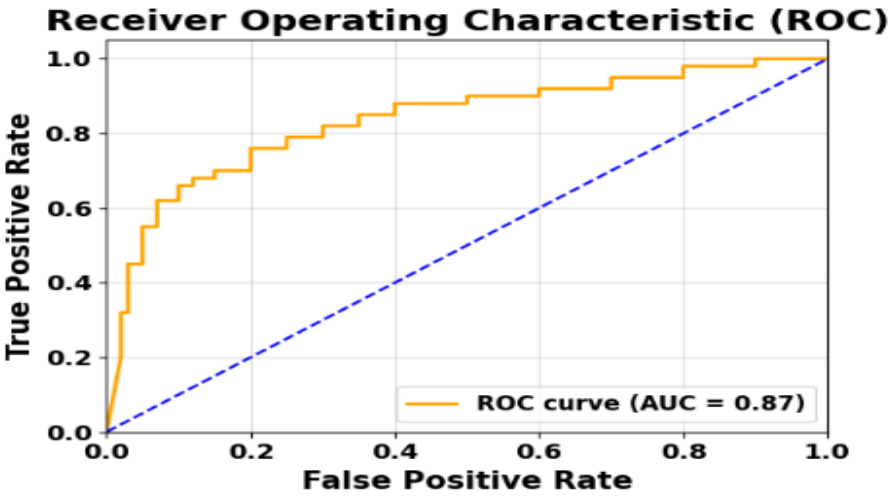


**Fig. 11 ROC curve of Custom CNN**

Fig. 8. shows the strong performance of the suggested Hybrid VGG16 + SVM model optimized using the Dandelion Optimizer (DO), which achieved an AUC of 0.99, with the ROC curve climbing almost vertically from the origin and closely following the plot's top border. The trend shows perfect sensitivity and specificity through all measured thresholds. The system achieves outstanding classification performance because it combines VGG16 feature extraction with SVM classification and DO-based hyperparameter tuning, allowing the optimizer to discover the best settings for differentiating between benign and can-cerous samples. An AUC of 0.92 was shown by the ROC curve for DenseNet121 in Fig. 9. With a false positive rate (FPR) of 0.1 and a true positive rate (TPR) of around 0.9, the model showed an initial rapid rise. The system demonstrates strong ability to separate different classes although its performance falls short of the recommended system. Fig.10. depicts ResNet-50's performance, which had an AUC of 0.89 and showed a quick initial climb to 0.9 TPR at FPR = 0.1, after which the curve flattened, showing a reasonable trade-off between detection sensitivity and false positive control. The custom CNN model achieved its lowest AUC score of 0.87 according to Fig.11., which shows the model's ROC analysis. The system reached only 0.6 TPR at FPR 0.1 before showing gradual improvement, which demonstrated its weak ability to distinguish between different classes. The VGG16 + SVM + DO framework shows superior performance because its ROC analysis demonstrates better separation of classes at different thresholds. The DO-based optimization method has proven to enhance diagnostic accuracy according to its successful implementation in this research project.

### 5.3 Performance Matrix

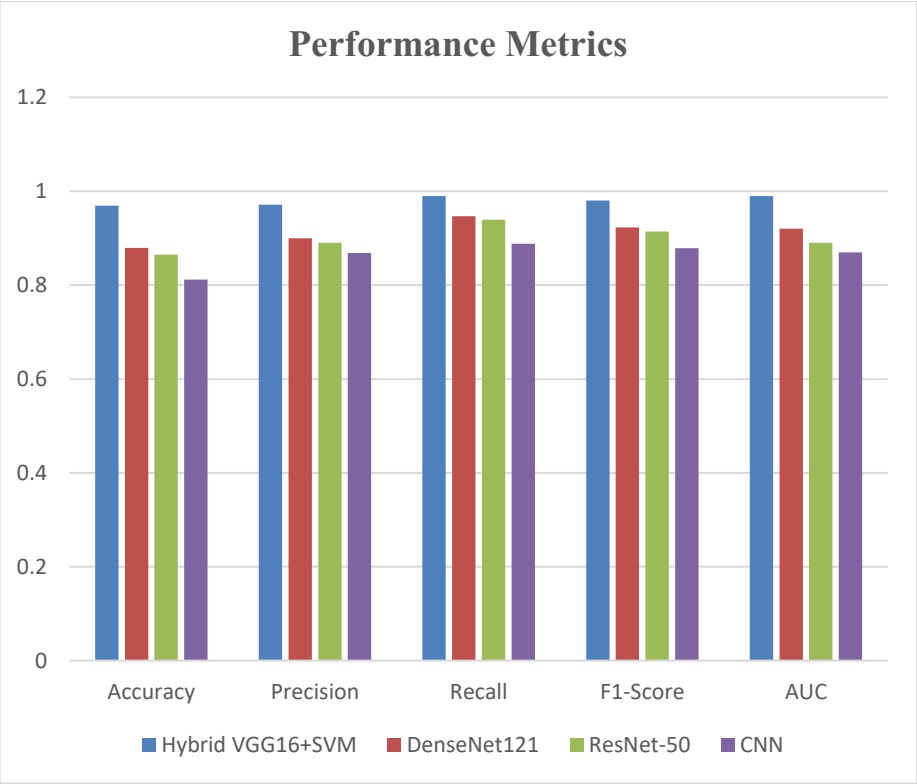


**Fig. 12 Performance comparison across for all models.**

The proposed hybrid VGG16+SVM model, which combines deep features extracted from the VGG16 convolutional neural network that is optimized using a Support Vector Machine Dandelion Optimizer, was compared to three baseline models for multimodal lung cancer classification: The three networks shown in Fig.12. are DenseNet121, ResNet-50, as well as a regular CNN. With an F1-score of 0.9802, a recall rate of 0.9895, an accuracy rate of 0.9694, and a precision rate of 0.9711, the hybrid VGG16+SVM model performed well across the board. When applied to multimodal data sets that included histology, transcriptomic, and proteomic information, the technique showed an enhanced ability to distinguish between cancerous and noncancerous instances. In contrast, DenseNet121 outperformed ResNet-50 in the following metrics: recall (0.865), F1-score (0.939), accuracy (0.890), precision (0.947), and F1-score (0.923). Conventional CNN performed poorly with a recall of 0.8884, F1-score of 0.8783, accuracy of 0.8116, as well as precision of 0.8683. In the hybrid model, the superior results can be attributed to its effective fusion of deep VGG16 features with the SVM's nonlinear classification capabilities, which are enhanced by optimal hyperparameter tuning, allowing it to outperform deeper architectures like DenseNet121 and ResNet-50, which

may struggle with the complexity of multimodal data, and the simpler CNN, which lacks sufficient feature extraction depth.

The assessment of various data types impact on total classification accuracy presents its results through Table 6. The multimodal fusion method demonstrates superior performance to both image-only and omics-only input types throughout all testing metrics because it achieves maximum accuracy results of 0.9661 and AUC score of 0.981. The research shows that histopathological data combined with molecular data produces better feature representation while multimodal learning enables models to generalize better through its integration of different biomedical data sources.

**Table 6.** Performance Across Different Data Modalities

| **Input Type** | **Accuracy** | **Precision** | **Recall** | **F1-Score** | **AUC** |
|---|---|---|---|---|---|
| Histopath image (LungHist700) | 0.912 | 0.925 | 0.95 | 0.9373 | 0.94 |
| CSV Only (RNA-sequence,) | 0.885 | 0.9 | 0.92 | 0.91 | 0.91 |
| **Multi-modal(LungHist700 histopathology + RNA-Seq)** | **0.9661** | **0.9702** | **0.9883** | **0.9791** | **0.981** |

**Table 7. Performance Comparison of Hyperparameter Optimization Techniques**

| **Optimization Method** | **Accuracy** | **Precision** | **Recall** | **F1-Score** | **AUC** |
|---|---|---|---|---|---|
| Particle Swarm Optimization (PSO) | 0.951 | 0.957 | 0.974 | 0.9654 | 0.97 |
| Genetic Algorithm (GA) | 0.952 | 0.958 | 0.975 | 0.9664 | 0.97 |
| Grey Wolf Optimizer (GWO) | 0.956 | 0.962 | 0.978 | 0.9699 | 0.97 |
| **Dandelion optimizer (DO)** | **0.9602** | **0.9665** | **0.9856** | **0.9729** | **0.978** |

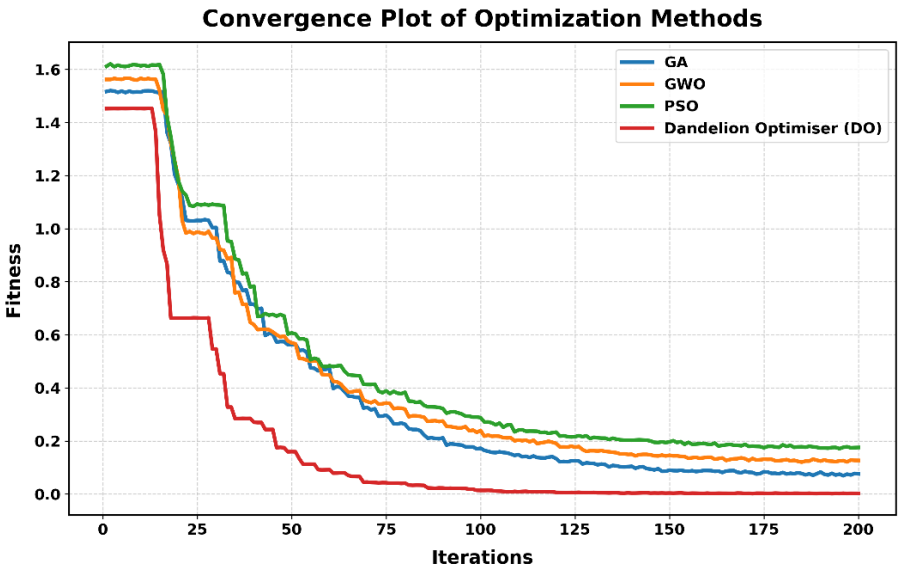


**Fig. 13 Convergence plot comparison of proposed method with multiple optimizers**.

In addition to investigating how different forms of data impact the proposed Dandelion optimizer (DO), the performance of numerous hyperparameter optimization methodologies is compared. According to Table 7, the suggested DO consistently outperforms other popular optimization techniques as Particle Swarm Optimization (PSO), Genetic Algorithm (GA), and Grey Wolf optimizer (GWO). These techniques perform competitively owing to their global search capabilities; nonetheless, DO obtains the accuracy of 0.9602 and AUC of 0.978. This increase is mostly due to its adaptive exploration-exploitation method, which speeds up convergence and improves the capacity to locate ideal hyperparameters for the SVM classifier.

The suggested system performs well and consistently in lung cancer categorization by combining histopathological, transcriptomic, proteomic, and clinical data. The DO-optimized hybrid VGG16-SVM model outperforms unimodal methods and other optimization techniques in terms of predictive performance. These findings show that combining deep feature extraction with appropriately adjust-ed machine learning classifiers is a dependable and successful technique for multimodal biomedical data processing. Fig. 13. shows the convergence behavior of PSO, GA, GWO, and the suggested DO during SVM hyperparameter optimization. All optimization approaches show a monotonically declining trend in fitness values over iterations, showing a gradual increase in solution quality. However, their convergence properties are very different. The suggested DO has the quickest convergence rate, with a rapid fall in fitness values during early iterations, followed by stabilization at a lower optimum than other approaches. GWO has a modest convergence speed, outperforms PSO and GA, but requires more iterations to achieve stability. In contrast, PSO and GA show slower con-vergence, with

progressive fitness decrease and delayed stabilization. Further-more, DO achieves earlier convergence, implying better search efficiency and quicker discovery of optimum hyperparameter areas. This behavior demonstrates the success of DO's adaptive exploration-exploitation technique, which allows for a better balanced and directed search process. Overall, the convergence study shows that the Dandelion optimizer beats the other optimization methodologies.

## 6 Discussions

A model that combines VGG16 with SVM is suggested, optimized with the Dandelion optimizer (DO), outperforms the LungHist700 dataset in classifying malignant versus non-cancerous lung histology, in a 5-fold cross-validation mean All the numbers add up to a very respectable 0.9694 accuracy, 0.9711 precision, 0.9895 recall, 0.9802 F1-score, and 0.99 AUC, as shown in Table 4f. All of the baseline models, including ResNet-50, DenseNet121, and a regular CNN, are outperformed by these findings. The average accuracy, precision, recall, and F1-score for the conventional CNN were 0.8116, 0.8683, 0.8884, and 0.85, respectively. Based on the per-fold performance parameters, ResNet-50 achieved an average accuracy of 0.865, precision of 0.890, recall of 0.939, F1-score of 0.914, as well as AUC of 0.89. The model addresses key challenges in previous lung cancer classification research by integrating VGG16-derived histological em-beddings with transcriptomic and proteomic profiles, as well as applying stain normalization via the Macenko method and patch-level filtering, such as overfit-ting on small, high-dimensional biomedical datasets, noise and missing values in multimodal omics data, and inefficient hyperparameter tuning. The dual-stage optimization strategy, combining GridSearchCV's exhaustive search with DO's bio-inspired approach, utilizes dandelion seed dispersal to balance exploration and exploitation. It efficiently tunes SVM hyperparameters (C, γ) via 5-fold cross-validation accuracy, reducing computational costs and avoiding local optima. The technique enables better generalization and model understanding com-pared to black-box deep learning models which experience bias and face challenges in medical implementation. The system achieves its distinctive quality through the combined power of multimodal feature fusion and DO-based optimization methods which enable it to surpass existing unimodal and basic hybrid CNN-SVM systems by identifying cancer diversity and controlling nonlinear decision boundaries. The model's system shows consistent accuracy through measurements, establishing it as a new benchmark for lung cancer diagnosis that maintains both interpretable results and accurate performance across large bio-medical datasets.

## 7 Conclusion

The study presents a Hybrid VGG16-Support Vector Machine (SVM) model which underwent optimization through Dandelion optimizer (DO) to achieve precise detection of malignant and non-cancerous lung histology. The proposed approach uses VGG16

for deep histological feature extraction together with multimodal omics data which includes transcriptome and proteomic profiles to create a comprehensive cancer heterogeneity assessment. Stain normalization and patch-level filtering improve the quality and consistency of histological inputs by addressing issues including noise, missing values, and overfitting on high-dimensional biomedical datasets. The Dandelion optimizer performs three functions which make it necessary for this system because it optimizes SVM hyperparameters and achieves a balance between exploration and exploitation while preventing the system from reaching local optimal solutions. Bio-inspired optimization techniques enable the model to maintain its resilience and interpretability because they exceed the limitations of conventional black-box deep learning methods, which makes the model suitable for use in clinical environments. This study mostly adds value by bringing together multimodal feature fusion with DO-based optimization, such that the model can identify various lung cancer data with complicated nonlinear correlations. The current method outperforms earlier unimodal and basic hybrid CNN-SVM systems because it achieves decision boundary optimization while maintaining system scalability and decision-making transparency. The Hybrid VGG16-SVM model produces reliable results for lung cancer diagnosis because its accuracy shows consistent performance during testing across all validation segments. The research demonstrates that using deep learning histology embed-dings together with multimodal omics data and effective DO optimization methods, will pro-duce significant improvements in diagnostic accuracy and clinical results. This method establishes a new standard for lung cancer classification because it demonstrates effective results with complex biomedical datasets, while creating a research foundation for AI-based diagnostic systems, which enable interpretable results in various cancer types and high-dimensional biomedical data.

**Acknowledgments**. The authors would like to express their sincere gratitude to all individuals and institutions that contributed to the successful completion of this research. Special thanks are extended to the providers of the LungHist700 Dataset for making high-quality histopathological data publicly available, which significantly supported the experimental validation of this study. The authors also acknowledge the support of their respective aca-demic and research institutions for providing the necessary computational resources and infrastructure required to carry out this work.

**Disclosure of Interests**. The authors declare that they have no competing interests to dis-close that are relevant to the content of this article.t

## References

1. J. Zhou, Y. Xu, J. Liu, L. Feng, J. Yu, and D. Chen, “Global burden of lung cancer in 2022 and projections to 2050: Incidence and mortality estimates from GLOBOCAN,” Cancer Epidemiol., vol. 93, p. 102693, 2024.
2. C. Li et al., “Global burden and trends of lung cancer incidence and mortality,” Chin. Med. J. (Engl)., vol. 136, no. 13, pp. 1583–1590, 2023.

3. H. Sung et al., “Global cancer statistics 2020: GLOBOCAN estimates of incidence and mortality worldwide for 36 cancers in 185 countries,” CA. Cancer J. Clin., vol. 71, no. 3, pp. 209–249, 2021.
4. G. Stamatis, W. Eberhard, and C. Pöttgen, “Surgery after multimodality treatment for non-small-cell lung cancer,” Lung Cancer, vol. 45, pp. S107–S112, 2004.
5. A. J. Scott et al., “Diagnostic accuracy of computer-aided detection during active case finding for pulmonary tuberculosis in Africa: a systematic review and meta-analysis,” in Open forum infectious diseases, Oxford University Press US, 2024, p. ofae020.
6. K. Ma, M. Zheng, W. Chen, Y. Qi, and H. Rong, “Research progress in computer-aided diagnosis systems for lung cancer,” npj Digit. Med., vol. 8, no. 1, p. 722, 2025.
7. A. C. Pacurari et al., “Diagnostic accuracy of machine learning AI architectures in detection and classification of lung cancer: a systematic review,” Diagnostics, vol. 13, no. 13, p. 2145, 2023.
8. S. S. Yadav and S. M. Jadhav, “Deep convolutional neural network based medical image classification for disease diagnosis,” J. Big data, vol. 6, no. 1, pp. 1–18, 2019.
9. X. Jiang, Z. Hu, S. Wang, and Y. Zhang, “Deep learning for medical image-based cancer diagnosis,” Cancers (Basel)., vol. 15, no. 14, p. 3608, 2023.
10. B. K. Hatuwal and H. C. Thapa, “Lung cancer detection using convolutional neural network on histopathological images,” Int. J. Comput. Trends Technol, vol. 68, no. 10, pp. 21–24, 2020.
11. Y. Kumaran S, J. J. Jeya, S. B. Khan, S. Alzahrani, and M. Alojail, “Explainable lung cancer classification with ensemble transfer learning of VGG16, Resnet50 and InceptionV3 using grad-cam,” BMC Med. Imaging, vol. 24, no. 1, p. 176, 2024.
12. H. H. Zargar, S. H. Zargar, R. Mehri, and F. Tajidini, “Using VGG16 Algorithms for classification of lung cancer in CT scans Image,” arXiv Prepr. arXiv2305.18367, 2023.
13. V. Sreeprada and K. Vedavathi, “Lung cancer detection from X-Ray images using hybrid deep learning technique,” Procedia Comput. Sci., vol. 230, pp. 467–474, 2023.
14. I. W. B. Sentana, S. A. Asri, N. Jawas, and A. E. Wardani, “CNN and SVM Based Classifier Comparation to Detect Lung Nodule In Computed Tomography Images,” in International Conference on Science and Technology (ICST 2018), Atlantis Press, 2018, pp. 29–34.
15. E. Carrizosa, B. Martin-Barragan, and D. R. Morales, “A nested heuristic for parameter tuning in support vector machines,” Comput. Oper. Res., vol. 43, pp. 328–334, 2014.
16. D. P. Mishra, H. K. Gupta, G. Saajith, and R. Bag, “Optimizing heart disease prediction model with gridsearchCV for hyperparameter tuning,” in 2024 1st International Conference on Cognitive, Green and Ubiquitous Computing (IC-CGU), IEEE, 2024, pp. 1–6.
17. G. N. Ahmad, H. Fatima, S. Ullah, and A. S. Saidi, “Efficient medical diagnosis of human heart diseases using machine learning techniques with and without GridSearchCV,” Ieee Access, vol. 10, pp. 80151–80173, 2022.
18. R. Javed, T. Abbas, A. H. Khan, A. Daud, A. Bukhari, and R. Alharbey, “Deep learning for lungs cancer detection: a review,” Artif. Intell. Rev., vol. 57, no. 8, p. 197, 2024.
19. M. M. Rahman, M. K. Nasir, M. Nur-A-Alam, and M. S. I. Khan, “Proposing a hybrid technique of feature fusion and convolutional neural network for melanoma skin cancer detection,” J. Pathol. Inform., vol. 14, p. 100341, 2023, doi: https://doi.org/10.1016/j.jpi.2023.100341.
20. D. A. Ragab, M. Sharkas, S. Marshall, and J. Ren, “Breast cancer detection using deep convolutional neural networks and support vector machines,” PeerJ, vol. 7, p. e6201, 2019.
21. B. R. Sandhya, L. Anushree, R. M. Darshan, A. Kashyap, and K. Amogha, “High-Precision Detection of Lung Adenocarcinoma Using Augmented VGG16 and Transfer Learning,” Indian J. Sci. Technol., 2024.

22. V. K. Velpula, K. R. Reddy, K. N. Prakash, K. P. Jasmine, and V. Jyothi Sri, "Optimizing Brain Tumor Classification: Integrating Deep Learning and Machine Learning with Hyperparameter Tuning," 2025. doi: 10.3390/engproc2025087064.
23. M. Avanzo, J. Stancanello, G. Pirrone, and G. Sartor, "Radiomics and deep learning in lung cancer," Strahlentherapie und Onkol., vol. 196, pp. 879–887, 2020.
24. M. M. R. Sweet et al., "COMPARATIVE ANALYSIS OF MACHINE LEARNING TECHNIQUES FOR ACCURATE LUNG CANCER PREDICTION," Am. J. Eng. Technol., vol. 6, no. 09, pp. 92–103, 2024.
25. N. Kalaivani, N. Manimaran, D. S. Sophia, and D. D Devi, "Deep learning based lung cancer detection and classification," in IOP conference series: materials science and engineering, IOP Publishing, 2020, p. 12026.
26. D. Ardila et al., "End-to-end lung cancer screening with three-dimensional deep learning on low-dose chest computed tomography," Nat. Med., vol. 25, no. 6, pp. 954–961, 2019.
27. B. R. Pandit et al., "Deep learning neural network for lung cancer classification: enhanced optimization function," Multimed. Tools Appl., vol. 82, no. 5, pp. 6605–6624, 2023.
28. A. Priya and P. Shyamala Bharathi, "SE-ResNeXt-50-CNN: A deep learning model for lung cancer classification," Appl. Soft Comput., vol. 171, p. 112696, 2025, doi: https://doi.org/10.1016/j.asoc.2025.112696.
29. P. Wu, X. Sun, Z. Zhao, H. Wang, S. Pan, and B. Schuller, "Classification of lung nodules based on deep residual networks and migration learning," Comput. Intell. Neurosci., vol. 2020, no. 1, p. 8975078, 2020.
30. G. Zhang, Z. Yang, L. Gong, S. Jiang, and L. Wang, "Classification of benign and malignant lung nodules from CT images based on hybrid features," Phys. Med. Biol., vol. 64, no. 12, p. 125011, 2019.
31. T. Meeradevi, S. Sasikala, L. Murali, N. Manikandan, and K. Ramaswamy, "Lung cancer detection with machine learning classifiers with multi-attribute decision-making system and deep learning model," Sci. Rep., vol. 15, no. 1, p. 8565, 2025, doi: 10.1038/s41598-025-88188-w.
32. K. V. Aishwarya and A. Asuntha, "A survey on comparative study of lung nodules applying machine learning and deep learning techniques," Multimed. Tools Appl., vol. 84, no. 5, pp. 2127–2181, 2025, doi: 10.1007/s11042-024-20009-0.
33. H. Dawood, M. Nawaz, M. U. Ilyas, T. Nazir, and A. Javed, "Attention-guided CenterNet deep learning approach for lung cancer detection," Comput. Biol. Med., vol. 186, p. 109613, 2025, doi: https://doi.org/10.1016/j.compbiomed.2024.109613.
34. D. Mannepalli, T. Kuan Tak, S. Bala Krishnan, and V. Sreenivas, "GSC-DVIT: A vision transformer based deep learning model for lung cancer classification in CT images," Biomed. Signal Process. Control, vol. 103, p. 107371, 2025, doi: https://doi.org/10.1016/j.bspc.2024.107371.
35. C. P. Maheswaran, B. N. Anand, T. S. P. Surya, and T. Sankeeth Ram, "Enhanced VGG16 model for detection and classification of lung cancer prediction," in AIP Conference Proceedings, AIP Publishing LLC, 2025, p. 50016.
36. N. Vasudeva, V. K. Sharma, P. Chauhan, and S. Awasthi, "Comparative Analysis of VGG16, InceptionV3 and ResNet50 for Lung Cancer Detection in Medical Imaging," in 2025 International Conference on Pervasive Computational Technologies (ICPCT), 2025, pp. 662–666. doi: 10.1109/ICPCT64145.2025.10940488.
37. N. N. Jafery, S. N. Sulaiman, M. K. Osman, N. K. Abdul Karim, Z. H. Che Soh, and N. A. Mat Isa, "Comparative Analysis of Hybrid 1D-CNN-LSTM and VGG16-1D-LSTM for Lung Lesion Classification," J. Electr. Eng. Technol., vol. 20, no. 4, pp. 2617–2630, 2025, doi: 10.1007/s42835-025-02182-w.

38. P. Nanglia, S. Kumar, A. N. Mahajan, P. Singh, and D. Rathee, “A hybrid algorithm for lung cancer classification using SVM and Neural Networks,” ICT Express, vol. 7, no. 3, pp. 335–341, 2021.
39. F. Maulidina, Z. Rustam, and J. Pandelaki, “Lung Cancer Classification using Support Vector Machine and Hybrid Particle Swarm Optimization-Genetic Algorithm,” in 2021 International Conference on Decision Aid Sciences and Application (DASA), 2021, pp. 751–755. doi: 10.1109/DASA53625.2021.9682259.
40. A. Y. Saleh et al., “Lung cancer medical images classification using hybrid,” 2021.
41. B. R. Manju, V. Athira, and A. Rajendran, “Efficient multi-level lung cancer prediction model using support vector machine classifier,” IOP Conf. Ser. Mater. Sci. Eng., vol. 1012, no. 1, p. 12034, 2021, doi: 10.1088/1757-899X/1012/1/012034.
42. P. M., R. V., B. V., and G. T., “Enhanced Prediction of Lung Cancer Stages using SVM and Medical Imaging,” in 2025 International Conference on Electronics and Renewable Systems (ICEARS), 2025, pp. 1334–1338. doi: 10.1109/ICEARS64219.2025.10941144.
43. N. K. Tiwari, A. Bajpai, V. Srivastava, S. Yadav, and N. Tiwari, “Integrating Pretrained CNN and SVM for Improved Lung Cancer Classification,” in 2024 IEEE 13th International Conference on Communication Systems and Network Technologies (CSNT), 2024, pp. 922–927. doi: 10.1109/CSNT60213.2024.10546020.
44. S. Mehta and A. Bhalla, “Hybrid Learning in Medical Imaging: CNN-SVM Applications in Lung Cancer Detection,” in 2025 International Conference on Automation and Computation (AUTOCOM), 2025, pp. 1412–1416. doi: 10.1109/AUTOCOM64127.2025.10957162.
45. V. Ahuja, T. S. Kehal, C. Rajesh, A. Dhiman, and L. Singla, “Deep Hybrid Models in Medical Imaging: CNN-SVM-Based Lung Cancer Detection with Statistical Insights,” in 2025 6th International Conference for Emerging Technology (INCET), IEEE, 2025, pp. 1–5.
46. M. S. Hossain, N. Basak, M. A. Mollah, M. Nahiduzzaman, M. Ahsan, and J. Haider, “Ensemble-based multiclass lung cancer classification using hybrid CNN-SVD feature extraction and selection method,” PLoS One, vol. 20, no. 3, p. e0318219, 2025.
47. S. Muthumarilakshmi et al., “A Novel Hybrid Neural Support Vector Algorithm for Lung Cancer Progression Prediction Using NN and SVM,” J. Neonatal Surg., vol. 14, no. 5, pp. 227–237, 2025.
48. J. Shrivastav and R. Pandey, “Enhanced Lung Cancer Detection Using a Hybrid AlexNet-CNN and Handcrafted Feature Fusion with mRMR Feature Selection and SSA-GWO Optimized Segmentation,” Int. J. Environ. Sci., vol. 11, no. 22, pp. 16–28, 2025.
49. P. Khabiya and F. Parwej, “MCNN-SVM : A Hybrid Deep Learning and SVM-Based Framework for Lung and Colon Cancer Image Classification,” J. Neonatal Surger, vol. 14, no. 21, pp. 1611–1624, 2025.
50. S. N. Yousafzai et al., “A hybrid deep learning approach integrating CNN and transformer for lung cancer classification using CT scans,” Sci. Rep., 2026.
51. G. Inbasakaran and J. A. Ruth, “Clinical-Ready CNN Framework for Lung Cancer Classification: Systematic Optimization for Healthcare Deployment with Enhanced Computational Efficiency,” Intell. Med., p. 100292, 2025.
52. X. Fu, R. Lin, W. Du, A. Tavares, and Y. Liang, “Explainable hybrid transformer for multi-classification of lung disease using chest X-rays,” Sci. Rep., vol. 15, no. 1, p. 6650, 2025, doi: 10.1038/s41598-025-90607-x.
53. L. Kamala and K. G. Mohan, “An efficient hybrid artificial intelligence framework for lung cancer classification using CT images,” Sci. Rep., 2025.
54. H. Yang, J. Ni, J. Gao, Z. Han, and T. Luan, “A novel method for peanut variety identification and classification by Improved VGG16,” Sci. Rep., vol. 11, no. 1, pp. 1–17, 2021, doi: 10.1038/s41598-021-95240-y.

55. S. Tammina, “Transfer learning using VGG-16 with Deep Convolutional Neural Network for Classifying Images,” Int. J. Sci. Res. Publ., vol. 9, no. 10, p. p9420, 2019, doi: 10.29322/ijsrp.9.10.2019.p9420.
56. J. Brank, M. Grobelnik, N. Milic-Frayling, and D. Mladenic, “Feature selection using linear support vector machines,” 2002.
57. C. Cortes and V. Vapnik, “Support-vector networks,” Mach. Learn., vol. 20, pp. 273–297, 1995.
58. E. Eker, “Development of random walks strategy-based dandelion optimizer and its application to engineering design problems,” IEEE Access, vol. 13, pp. 56547–56575, 2025.
59. H. D. Nguyen and L. H. Pham, “Solutions of economic load dispatch problems for hybrid power plants using Dandelion optimizer,” Bull. Electr. Eng. Informatics, vol. 12, no. 5, pp. 2569–2576, 2023.
60. Y. Fujii et al., “Effectiveness of data-augmentation on deep learning in evaluating rapid on-site cytopathology at endoscopic ultrasound-guided fine needle aspiration,” Sci. Rep., vol. 14, no. 1, p. 22441, 2024, doi: 10.1038/s41598-024-72312-3.
61. J. Diosdado, P. Gilabert, S. Seguí, and H. Borrego, “LungHist700: A dataset of histological images for deep learning in pulmonary pathology.,” Sci. data, vol. 11, no. 1, p. 1088, Oct. 2024, doi: 10.1038/s41597-024-03944-3.
62. J. M. Dolezal et al., “Slideflow: deep learning for digital histopathology with real-time whole-slide visualization,” BMC Bioinformatics, vol. 25, no. 1, p. 134, 2024, doi: 10.1186/s12859-024-05758-x.